Anal. Chem. **2006,** *78,* 2009−2018

Surface Plasmon Resonance Imaging of Biomolecular Interactions on a Grating-Based Sensor Array

Bipin K. Singh and Andrew C. Hillier*

Department of Chemical Engineering and Department of Chemistry, Iowa State University, Ames, Iowa 50011

A surface plasmon resonance sensor array based upon a grating substrate was developed for the detection of biomolecular interactions. The substrate consisted of a gold grating prepared by wet chemical treatment of a commercial recordable compact disk. A custom-built floating pin microspotter was constructed to deliver solutions containing ω-functionalized linear alkanethiols to the grating surface and produce an array of sensor elements with different exposed functional end groups. This array platform can be used to study biomolecular interactions in a label-free, sensitive, and high-throughput format. To illustrate the performance of this device, a test protein (bovine serum albumin) was exposed to sensor elements containing an array of functionalized alkanethiols possessing either activated carboxylic acid-, amine-, or hydroxyl-terminated regions. Local changes in plasmon resonance were monitored in a fixed-angle imaging configuration. Plasmon images clearly distinguish the degree of protein attachment at the various surfaces. The molecular binding events on the grating were also confirmed by ellipsometry. This grating-based SPR imaging platform represents a simple and robust method for performing label-free, high-sensitivity, and high-throughput detection of biomolecular interactions.

Surface plasmon resonance (SPR) sensing has emerged as a powerful tool to measure the binding of analytes to functionalized surfaces and immobilized (bio)molecules and has found utility in the development of immunosensors,[1−3] proteomics,[4,5] drug discovery,[6,7] immunogenicity studies,[8,9] and detection of environmental pollutants[10] and food contaminants.[11] It has also been used to monitor such events as DNA hybridization[12,13] and protein−DNA interactions.[14,15] Several reviews are available in the literature regarding surface plasmon resonance sensing.[14,16−19] The advantages that SPR sensing provides over competing techniques for measuring biomolecular interactions such as radioimmunoassay and enzyme-linked immunosorbent assay include that it requires very low reagent quantities, obviates the need for labeling or complex reaction/washing steps, and can be performed in real time with high precision and specificity of the assay.[20] In addition, the ability to perform SPR imaging makes this technique a promising high-throughput screening tool.

To achieve high-throughput SPR sensing, one can increase the number of sensor elements per unit area by miniaturization or by the creation of sensor arrays. The use of microfluidic channels has been demonstrated for the study of antibody/antigen interactions at varying concentration levels as a one-dimensional array.[21] Two-dimensional array-based SPR sensing platforms have also been reported for a range of biological analytes.[22−29]

* To whom correspondence should be addressed. E-mail: hillier@iastate.edu.

(1) Nishimura, T.; Hifumi, E.; Fujii, T.; Niimi, Y.; Egashira, N.; Shimizu, K.; Uda, T. *Electrochemistry* **2000**, *68*, 916−919.
(2) Hsieh, H. V.; Stewart, B.; Hauer, P.; Haaland, P.; Campbell, R. *Vaccine* **1998**, *16*, 997−1003.
(3) Mullett, W. M.; Lai, E. P. C.; Yeung, J. M. *Methods* **2000**, *22*, 77−91.
(4) Oda, Y.; Owa, T.; Sato, T.; Boucher, B.; Daniels, S.; Yamanaka, H.; Shinohara, Y.; Yokoi, A.; Kuromitsu, J.; Nagasu, T. *Anal. Chem.* **2003**, *75*, 2159−2165.
(5) Wilkinson, F. L.; Holaska, J. M.; Zhang, Z. Y.; Sharma, A.; Manilal, S.; Holt, I.; Stamm, S.; Wilson, K. L.; Morris, G. E. *Eur. J. Biochem.* **2003**, *270*, 2459−2466.
(6) Rich, R. L.; Day, Y. S. N.; Morton, T. A.; Myszka, D. G. *Anal. Biochem.* **2001**, *296*, 197−207.
(7) Baird, C. L.; Courtenay, E. S.; Myszka, D. G. *Anal. Biochem.* **2002**, *310*, 93−99.
(8) Smith, E. A.; Corn, R. M. *Appl. Spectrosc.* **2003**, *57*, 320A−332A.
(9) Carnahan, J.; Wang, P.; Kendall, R.; Chen, C.; Hu, S.; Boone, T.; Juan, T.; Talvenheimo, J.; Montestruque, S.; Sun, J. L.; Elliott, G.; Thomas, J.; Ferbas, J.; Kern, B.; Briddell, R.; Leonard, J. P.; Cesano, A. *Clin. Cancer Res.* **2003**, *9*, 3982S-3990S.
(10) Rodriguez-Mozaz, S.; Marco, M. P.; de Alda, M. J. L.; Barcelo, D. *Anal. Bioanal. Chem.* **2004**, *378*, 588−598.
(11) Baeumner, A. J. *Anal. Bioanal. Chem.* **2003**, *377*, 434−445.
(12) Nilsson, P.; Persson, B.; Uhlen, M.; Nygren, P. A. *Anal. Biochem.* **1995**, *224*, 400−408.
(13) Peterlinz, K. A.; Georgiadis, R. M.; Herne, T. M.; Tarlov, M. J. *J. Am. Chem. Soc.* **1997**, *119*, 3401−3402.
(14) Silin, V.; Plant, A. *Trends Biotechnol.* **1997**, *15*, 353−359.
(15) Gotoh, M.; Hasebe, M.; Ohira, T.; Hasegawa, Y.; Shinohara, Y.; Sota, H.; Nakao, J.; Tosu, M. *Genet. Anal.-Biomol. Eng.* **1997**, *14*, 47−50.
(16) Green, R. J.; Frazier, R. A.; Shakesheff, K. M.; Davies, M. C.; Roberts, C. J.; Tendler, S. J. B. *Biomaterials* **2000**, *21*, 1823−1835.
(17) Lechuga, L. M.; Calle, A.; Prieto, F. *Quim. Anal.* **2000**, *19*, 54−60.
(18) Homola, J.; Yee, S. S.; Gauglitz, G. *Sens. Actuators, B* **1999**, *54*, 3−15.
(19) Homola, J. *Anal. Bioanal. Chem.* **2003**, *377*, 528−539.
(20) Revoltella, R. P.; Robbio, L. L.; Liedberg, B. *Biotherapy* **1998**, *11*, 135−145.
(21) Berger, C. E. H.; Beumer, T. A. M.; Kooyman, R. P. H.; Greve, J. *Anal. Chem.* **1998**, *70*, 703−706.
(22) Thiel, A. J.; Frutos, A. G.; Jordan, C. E.; Corn, R. M.; Smith, L. M. *Anal. Chem.* **1997**, *69*, 4948−4956.
(23) Lee, H. J.; Goodrich, T. T.; Corn, R. M. *Anal. Chem.* **2001**, *73*, 5525−5531.
(24) Nelson, B. P.; Grimsrud, T. E.; Liles, M. R.; Goodman, R. M.; Corn, R. M. *Anal. Chem.* **2001**, *73*, 1−7.
(25) Kanda, V.; Kariuki, J. K.; Harrison, D. J.; McDermott, M. T. *Anal. Chem.* **2004**, *76*, 7257−7262.
(26) Yuk, J. S.; Jung, S. H.; Jung, J. W.; Hong, D. G.; Han, J. A.; Kim, Y. M.; Ha, K. S. *Proteomics* **2004**, *4*, 3468−3476.
(27) Shumaker-Parry, J. S.; Zareie, M. H.; Aebersold, R.; Campbell, C. T. *Anal. Chem.* **2004**, *76*, 918−929.

10.1021/ac0519209 CCC: $33.50
Published on Web 01/21/2006

A variety of schemes have been employed to excite surface plasmons, including the use of prisms and gratings,[18,19,28] as well as the recent discovery of surface plasmons excited by subwavelength features.[30,31] In the majority of SPR applications, the prism-based Kretschmann configuration is used for optical excitation of surface plasmons in a thin metal film under conditions of attenuated total internal reflection.[18] In this arrangement, light travels through the prism to excite plasmons in a thin metal film from the backside of the test sample. Thus, attenuation and optical artifacts due to the sample environment are avoided. However, only films of a precise and limited range of thickness may be used. An alternative form of excitation involves placing a sample directly onto a topographically modulated surface such as a grating and exciting surface plasmons by direct illumination.[32] The advantages of grating-based SPR sensing include the fact that a prism is not necessary to excite surface plasmons and the optical quality of the substrate is not crucial. In addition, the narrow window of thicknesses allowed for the metal film in the Kretschmann configuration is obviated with grating excitation. The use of external reflection with a grating substrate allows macroscopically thick metal films to be interrogated. Another appealing feature of grating-based SPR is that inexpensive and disposable plastic gratings can be used as substrates. For example, commercially available compact disks (CDs) and digital versatile disks (DVDs), which are mass produced by injection-molding techniques, can serve as inexpensive grating substrates. The presence of a pregroove (vide infra) in CD-Rs has motivated their use in SPR sensing. Indeed, the use of a gold grating from a commercial CD-R for excitation of surface plasmons was recently reported.[33] In addition, silver and gold CD-Rs have been used as a source of planar electrodes[34−36] and as a platform for the construction of alkanethiolate monolayers.[37] One limitation of grating-based SPR sensing is that, for in situ SPR studies, the solution should be transparent and interact minimally with the incident light. However, there is no such restriction if SPR detection is done in air, which makes it suitable for portable field testing applications and as a label-free tool for readout of DNA and protein microarrays.[38]

In this report, we describe the development of a grating-based sensor array for surface plasmon resonance imaging of biomolecular adsorption. A commercial CD-R is modified by chemical treatment and subsequent spot printing to create an array of carboxylic acid-, amine-, and hydroxyl-terminated self-assembled monolayer regions on gold. The binding of bovine serum albumin (BSA) is then interrogated by SPR imaging. Images depicting changes in SPR intensity at a fixed angle of incidence were captured to illustrate variations in BSA coverage versus position. Differences in BSA binding to carboxylic acid-, amine-, and hydroxyl-terminated regions are observed as well as significant nonspecific adsorption onto unmodified gold. This work demonstrates the utility and flexibility of this sensing technique as well as a discussion of some of the design issues associated with the grating geometry and sensor assembly.

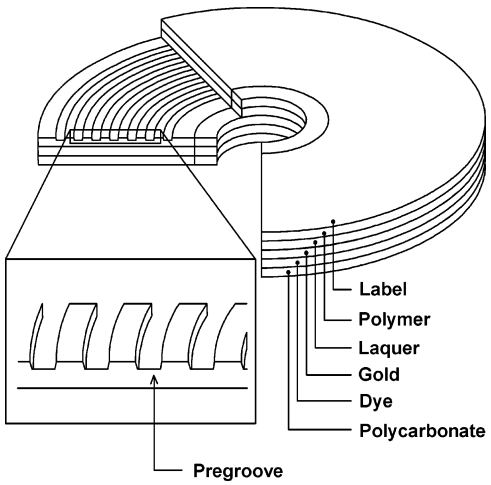

Figure 1. Diagram illustrating various layers of a commercial CD-R. The pregroove is stamped onto the polycarbonate substrate and coated with sequential layers of dye, gold, lacquer, polymer, and label.

EXPERIMENTAL SECTION

Materials and Reagents. Absolute ethanol, 11-mercaptoundecanoic acid (MUA), 11-merapto-1-undecanol (MUL), 11-amino-1-undecanethiol hydrochloride (MUN), BSA, *N*-hydroxysuccinimide (NHS), *N*-(3-dimethylaminopropyl)-*N*′-ethylcarbodiimide hydrochloride (EDC), and HEPES were purchased from Sigma-Aldrich (St. Louis, MO). Glycerol and sodium chloride were acquired from Fisher Scientific (Fairlawn, VA), and nitric acid was from J. T. Baker (Phillipsburg, NJ). All chemicals and reagents were used as received. Recordable compact disks (MAM-A Gold CD-R) were purchased from Inkjet Art Solutions (Salt Lake City, UT). Gold (99.999%) was purchased from Ernest Fullam (Latham, NY). HEPES-buffered saline (HBS, 10 mM HEPES, 150 mM sodium chloride) was prepared with the pH adjusted to 7.4 using 10 mM NaOH and stored at 4 °C. All buffers and solutions were prepared with 18 MΩ deionized water (NANOPure, Barnstead, Dubuque, IA). Solutions containing 10 mM MUA, MUN and MUL were made in glycerol and sonicated for 1 h prior to use.

Grating Construction. The CD-Rs used in this work consisted of sequential layers of polycarbonate, dye, gold, protective lacquer, and polymer coatings (Figure 1). In commercial CD-Rs, the polycarbonate layer has a spiraling groove (called a pregroove) formed during the injection molding process that assists in laser tracking during writing and recovery of data. A photosensitive dye is coated on top of this substrate, and it is this layer that is "burned" in the process of writing data on a CD-R. A thin (50−100 nm) layer of metal (e.g., gold) is sputtered on top of this dye followed by protective coats of lacquer and a polymer to prevent the metal film from damage. We took advantage of the fact that the pitch of the pregroove in CD-Rs is sufficient to excite surface plasmons on gold in air.

(28) Brockman, J. M.; Nelson, B. P.; Corn, R. M. *Annu. Rev. Phys. Chem.* **2000**, *51*, 41−63.
(29) Brockman, J. M.; Fernandez, S. M. *Am. Lab.* **2001**, *33*, 37.
(30) Brolo, A. G.; Gordon, R.; Leathem, B.; Kavanagh, K. L. *Langmuir* **2004**, *20*, 4813−4815.
(31) Barnes, W. L.; Dereux, A.; Ebbesen, T. W. *Nature* **2003**, *424*, 824−830.
(32) Raether, H. *Surface plasmons on smooth and rough surfaces and on gratings*; Springer-Verlag: Berlin, 1988.
(33) Fontana, E. *Appl. Opt.* **2004**, *43*, 79−87.
(34) Richter, E. M.; Augelli, M. A.; Magarotto, S.; Angnes, L. *Electroanalysis* **2001**, *13*, 760−764.
(35) Richter, E. M.; de Jesus, D. P.; Neves, C. A.; do Lago, C. L.; Angnes, L. *Quim. Nova* **2003**, *26*, 839−843.
(36) Angnes, L.; Richter, E. M.; Augelli, M. A.; Kume, G. H. *Anal. Chem.* **2000**, *72*, 5503−5506.
(37) Yu, H. Z. *Anal. Chem.* **2001**, *73*, 4743−4747.
(38) Yuk, J. S.; Ha, K. S. *Exp. Mol. Med.* **2005**, *37*, 1−10.

Further preparation of the CD-Rs involved removing the protective polymer and lacquer layers on the topside of the gold layer by a straightforward wet chemical treatment.[36] Briefly, pieces from CD-R were cut to size and then immersed in concentrated nitric acid for 4 min. The protective polymer and lacquer layers spontaneously delaminated to expose the gold grating, which was then washed several times with water and ethanol followed by drying with a nitrogen stream. The polycarbonate and gold surfaces were not damaged by this treatment. The gold surface was then cleaned in an oxygen plasma for 1 min to remove any residual organic impurities (plasma cleaner PDC-32G, Harrick Scientific, Ossining, NY). Freshly prepared gratings were typically used for each experiment.

Atomic Force Microscope (AFM) Imaging. AFM images of the various grating surfaces were acquired with a Dimension 3100 scanning probe microscope and Nanoscope IV controller (Veeco Metrology, LLC, Santa Barbara, CA). Imaging was performed in tapping mode using silicon TESP7 AFM tips (Veeco Metrology, LLC) with a spring constant of ~70 N m^{-1} and a resonance frequency of ~280 kHz.

Solid Pin Microspotter. A custom-built, floating pin microspotter was developed for construction of sensor arrays. Complete details of the design and performance of this spotting system will be the subject of a later report. Briefly, the microspotter consisted of a floating solid pin attached to a computer-controlled positioning system. Samples were placed beneath the floating pin near to a multiwell plate, which was used for reagent storage and sampling. The spotting pin consisted of a 229-μm-diameter stainless steel solid pin (V&P Scientific) attached to a mount that allowed the pin to float during contact with the surface to be printed. The floating feature allowed a constant force to be applied during printing, as dictated by the weight of the pin. The positioning system consisted of a motor driver (UNIDRIV6000, Newport Corp., Irvine, CA) connected to three integrated stepper motor/linear translation stages (ILS Series, Newport Corp.) assembled in an orthogonal fashion to provide three independent directions of motion. The motor driver was interfaced via a motion controller card (ESP6000, Newport Corp.) to a personal computer. Spotter positioning was controlled with a custom-designed printing program written in LabView (National Instruments, Austin, TX). The sample platform consisted of an optical table (Newport Corp.) with a tilt stage. A combination of a sample mount and a holder for a multiwell plate was attached to the tilt stage. The multiwell plate served as a storage container for the various reagents used in deposition and rinsing of the floating pint. Printing solutions typically contained a 10 mM concentration of the molecule of interest dissolved in glycerol. During formation of a single printed spot, the pin was immersed into the printing solution to a depth of ~100 μm and then positioned over the desired sample location. The pin was brought into contact with the sample surface for a predetermined period of time and then removed. This process delivered a well-controlled droplet of glycerol containing the molecule of interest. Arrays of various chemistries were created by subsequently cleaning the pin by dipping into a rinse solution, moving to a new reagent well, dipping of the pin to collect this solution, and then repeating the spotting procedure on a new location of the sample. This entire procedure was automated with the various parameters, including dipping time, spot location, and surface pattern, input using a custom LabView program. In the examples contained herein, spots of MUA, MUN, and MUL were created in array patterns consisting of alternating spots or quadrants of spots with different chemistries. More complicated patterns with additional chemistries could be easily fabricated.

Following delivery of the glycerol droplets, the solution was allowed to react with the surface for a period of ~15 min. This reaction resulted in the formation of a self-assembled monolayer of the specific alkanethiol at the spot location. Spots were subsequently washed with copious amounts of ethanol and water and dried in a stream of nitrogen. Activation of carboxylic acid-terminated monolayers was achieved by exposing the sample to an aqueous solution containing 150 mM EDC and 30 mM NHS for 30 min. This reaction resulted in the formation of NHS-activated MUA regions, while it showed little effect on other surface regions. Subsequent attachment of BSA to the array surface was achieved by exposing the surface for 90 min to a 0.8 mg mL^{-1} solution of BSA in HBS. The sample was then washed with HBS and dried under nitrogen. All reactions were carried out in covered 3−5-mL Teflon vessels.

Imaging Surface Plasmon Resonance. A custom-built device was used to collect SPR imaging data. The apparatus consisted of a white light source (LS-1 Tungsten Halogen Light Source, Ocean Optics, Dunedin, FL) coupled to a narrow band-pass interference filter with a central wavelength of 632 nm and full width half-maximum (fwhm) of 10 nm (Newport Corp.). The emerging light was collimated with a convex lens having a focal length of 150 mm (Newport Corp.). The resulting beam passed through a linear polarizer before illuminating the grating sensor. The sample was mounted on a rotating tilt stage for manual alignment and rotation. Reflected light was focused onto a high-sensitivity monochrome CCD camera (EHDkamPro02, EHD Imaging GmbH) using a variable zoom lens (Zoom7000, Navitar). Images were captured with a frame-grabber card (Pinnacle Systems, Inc., Mountain View, CA) using commercially available software (Studio 8, Pinnacle Systems, Inc.). Typically, images were captured using both p-polarized and s-polarized light with the sample rotation near the minimum in surface plasmon intensity. The polarization state of light was switched between p- and s-states by simply rotating the linear polarizer. To calculate absolute intensities, the response of CCD was calibrated using several neutral density filters. A linear response resulted with ~18 pixel values giving a 10% change in intensity.

Ellipsometry and Variable-Angle Surface Plasmon Resonance. Measurement of ellipsometry or variable-angle SPR was achieved using an automated, multifunctional optical system (Multiskop, Optrel GbR). Ellipsometric data were acquired at a single wavelength (632.8 nm) with a beam diameter of ~0.6 mm in the PCSA configuration at 70° angle of incidence. Values of ellipsometric angles, Δ and Ψ, were translated into equivalent optical thicknesses using a three-medium model. Variable-angle surface plasmon resonance measurements were performed using the same instrument in variable-angle mode after removing the compensator. The laser and detector arms were rotated using a two-arm motorized goniometer with an angular resolution of 0.001°. A rotatable Glan-Thompson polarizer with an extinction ratio of 10^{-8} (Halle) was used to control the polarization state of the laser. Angle scans were captured using both p- and s-polarized

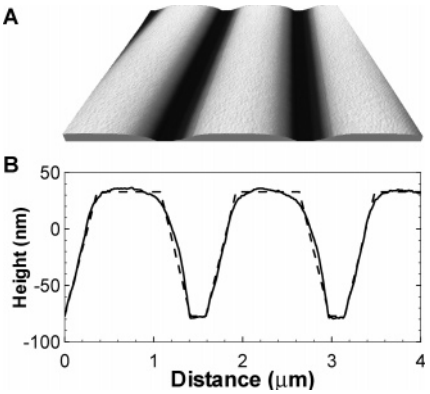

Figure 2. (A) AFM image (4 μm × 4 μm) of exposed gold layer on CD-R. (B) Cross-sectional profile (solid line) from the AFM scan and trapezoidal grating profile (dashed line) used for the simulations.

light reflected from the sample into a photodiode detector. The ratio of reflected p- and s-polarized light (R_p/R_s) was then calculated from these results.

RESULTS AND DISCUSSION

Samples were prepared by cutting pieces of the CD-R to size and then subjecting them to the wet chemical treatment (vide supra). Soaking a piece of CD-R in a concentrated nitric acid solution for 3−5 min was sufficient to remove the protective layers of lacquer and polymer from the surface of the gold layer. Optical transmission measurements indicated that the thickness of the gold layer was ∼70 nm. Atomic force microscopy images revealed a modulated structure (Figure 2A). Roughness analysis indicated a reasonably smooth gold surface with typical root-mean-squared roughness of ∼1.4 nm μm^{-2}. A cross-sectional profile perpendicular to the grating (Figure 2B) shows the longer-range topology of the surface with a period of 1560 nm and an amplitude of 115 nm. The shape of this surface profile approximates that of a trapezium with rounded corners.

Optical excitation of surface plasmons (SPs) at a metal−dielectric interface requires that the momentum of the incident light matches that of SPs in the metal. This occurs when the wavevector of incident light ($\boldsymbol{k}_x$) matches that of the SPs. The SPs have a wavevector ($\boldsymbol{k}_{sp}$), the real part of which is described by the following dispersion relation[32]

$$k'_{sp} = \frac{2\pi}{\lambda_0}\sqrt{\frac{\epsilon'_M \epsilon_D}{\epsilon'_M + \epsilon_D}} \qquad (1)$$

where λ_0 is the wavelength of excitation while ϵ_M ($= \epsilon'_M + i\epsilon''_M$) and ϵ_D are the dielectric constants of the metal and dielectric layers. Since the momentum of incident light in air is lower than that given by eq 1, a coupling device is needed. The most commonly used coupling involves use of a prism in the Kretschmann configuration. In this configuration, the momentum of light is increased due to the prism having a higher dielectric constant than air. Under conditions of total internal reflection, an evanescent wave is generated at the prism−metal interface, which then propagates and couples with SPs at the metal−dielectric surface.

Momentum can also be matched using metal diffraction gratings.[32] For a periodically modulated interface between a metal and a dielectric with a period Λ (Chart 1), the surface component of the wavevector of incident light can increase (or decrease) by integral multiples of the grating wavevector. If this increase matches that of SPs in the metal, it can couple to and excite them. Mathematically, this relationship can be expressed by

Chart 1. Schematic of Surface Plasmon Resonance on Gold Grating

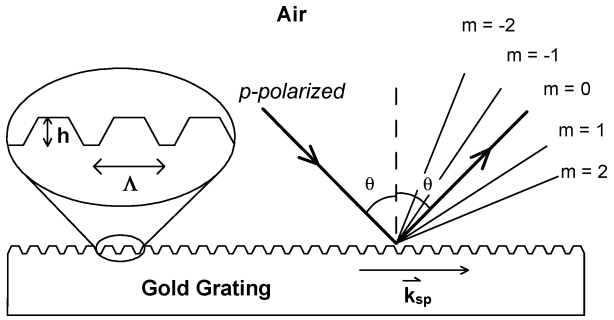

$$k'_{sp} = \frac{2\pi}{\lambda_0}\sqrt{\frac{\epsilon'_M \epsilon_D}{\epsilon'_M + \epsilon_D}} = \frac{2\pi}{\lambda_0}\sqrt{\epsilon_D}\sin\theta_0 + m\frac{2\pi}{\Lambda} = k'_x \qquad (2)$$

where θ_0 is angle of incidence and m is an integer (0, ±1, ±2, ...) indicating the diffracted order. For surface plasmons that propagate in the forward direction, the diffracted order of $m = +1$ will result in the strongest coupling.[39] When this coupling occurs, a sharp resonance dip is observed in the reflectance of p-polarized light.

To compare the SPR response of the commercial gratings used here to theoretical predictions, modeling was done using a commercial diffraction grating solver (PCGrate, International Intellectual Group, Inc., Penfield, NY). This solver uses an integral method to numerically solve the electromagnetism equations.[40] Results for several model surfaces along with an experimentally measured reflectivity profile for the gold-coated grating are shown in Figure 3. These curves depict relative reflectivity (R_p/R_s) versus angle of incidence for light at a wavelength of 632 nm. The experimental profile for the commercial CD-R grating shows a resonance dip with a minimum at 39.37°. Simulated curves are provided for gold surfaces having the same amplitude and period as measured from the CD-R grating, but with three different surface profiles: trapezoidal, triangular, and sinusoidal. In these simulations, the electric permittivity of air and gold was taken as 1 and −11.84 + i(1.36).[41] The general shape of all the curves is similar, but in all cases, the simulated results overestimate the measured angle of resonance minimum. The trapezoidal profile most closely captures the shape of the experimental curve. The difference between the simulated and experimental curves could arise from several factors. The biggest effect on the position of the resonance minimum is the pitch of the grating. For example, a decrease in the pitch by 25 nm would lower the predicted resonance minimum by 0.5°, which is enough to account for the differences between the simulated and experimental curves. The

(39) Pockrand, I.; Raether, H. *Opt. Commun.* **1976**, *18*, 395−399.
(40) Petit, R.; Botten, L. C. *Electromagnetic theory of gratings*; Springer-Verlag: Berlin, 1980.
(41) Innes, R. A.; Sambles, J. R. *J. Phys. F: Met. Phys.* **1987**, *17*, 277−287.

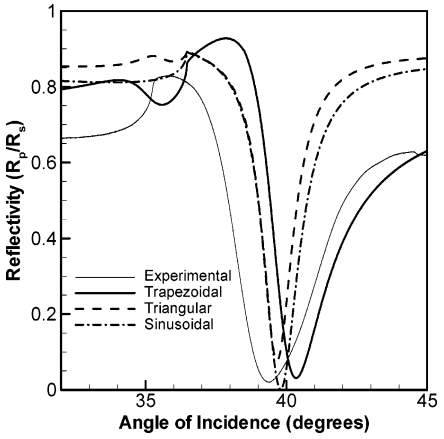

Figure 3. SPR curves as measured on grating at 632.8 nm (solid line) and as simulated with trapezoidal (bold solid line), triangular (dashed line), and sinusoidal (dash−dot line) grating profiles.

values input for the optical constants of gold in the simulation could also vary slightly from the true values exhibited by the gold-coated grating, but a sensitivity analysis indicated that these parameters did not have a significant effect on the value of the resonance minimum in the simulation. The thickness of the gold layer in these studies (∼50 nm) is such that it allows some light to pass through the grating, which could influence the response. Although there was some concern about the impact of the underlying phthalocyanine-based dyes used in these CD-Rs, they do not absorb light at the wavelength used for analysis.[42] Notably, prior work has shown that the gold surface prepared by a similar protocol behaves comparably to commercial gold electrodes in their electrochemical behavior[36,43] and also allows formation of self-assembled thiolate monolayers indistinguishable from those formed on evaporated gold.[37]

The gold gratings were subsequently modified to create a sensor array. Preparation of the sensing surface was achieved by functionalization of the gold using alkanethiols. A variety of surface functionalities can be readily fabricated on gold surfaces by tailoring the headgroup, X, of an ω-funcionalized n-alkanethiol, $HS-(CH_2)_n-X$ and allowing it to self-assemble on gold.[44,45] Similar self-assembly techniques have also been used to construct protein microarrays.[46] We chose MUA, MUL, and MUN to construct modified gold surfaces. MUA is a convenient choice for covalent coupling to proteins since NHS activation can be used to create a surface that will readily react with pendant primary amines.[47] MUL was chosen as a similarly sized control that presents a hydroxyl-terminated surface on gold, but is unaffected by the NHS treatment and, thus, should not covalently bind with proteins. MUN was also chosen as a similarly sized molecule that is not influenced by the NHS treatment but would provide a surface chemistry different from that of MUL. Two different sample types were used in the studies described here—patterned and unpatterned. Unpatterned samples were used for characterization with ellipsometry and variable-angle SPR scans, while the patterned samples were constructed as sensor arrays to be analyzed with SPR imaging.

The unpatterned samples were created by immersing the gold grating in a 10 mM solution of MUA, MUL, or MUN in glycerol for 15 min. After sequentially washing with ethanol and water and then drying with nitrogen, the samples were immersed in an aqueous NHS/EDC solution for 30 min. After a brief wash, the samples were blown dry with nitrogen and then immersed in a 0.5 mg/mL solution of BSA in HBS for 90 min. The samples were then rinsed with water, dried under nitrogen, and then immediately characterized.

Unpatterned samples were characterized at various stages of fabrication by variable angle SPR and ellipsometry. Angle scans of the reflectivity of p- and s-polarized light as well as ellipsometry measurements at a fixed angle of incidence were performed at the same spot on each sample. The samples were aligned so that the orientation of the gratings was perpendicular to the plane of incidence formed by the arms of the goniometer. This was achieved by ensuring that the diffracted reflections fell in the incidence plane of the laser arm. Reflectivity scans were recorded as a function of angle of incidence for p- and s-polarized light such that normalized reflectivity (R_p/R_s) could be plotted (Figure 4A). After completion of each reflectivity scan, a compensator was added to the instrument such that a null-ellipsometry measurement could be performed without disturbing the sample. Ellipsometric parameters were measured at 70° angle of incidence.

Figure 4A depicts SPR angle scans of the bare gold surface, after assembly of the MUA monolayer, following NHS ester formation, and after attachment of BSA to MUA. The three surface modification steps caused the SPR minimum to increase in intensity and shift toward progressively higher angles by 0.13°, 0.2°, and 0.4° with respect to the clean gold surface (Table 1). Ellipsometry measurements provided total film thickness values of 1.61, 1.76, and 5.54 nm for the MUA, MUA/NHS, and MUA/NHS/BSA layers, respectively. Alternatively, the individual film thicknesses for MUA, NHS, and BSA layers are 1.61, 0.15, and 3.78 nm. To calculate film thickness from ellipsometric parameters, a three-layer ambient-film−substrate model was used with a refractive index of 1.45 for the film.[48] Fitting the SPR curves to a thin-film model was not done due to computational limitations of the grating solver. Although modeling the results from a typical Kretschmann configuration is straightforward, solving the grating equations for a surface/film/ambient interface is much more complex and beyond the scope of this work. Therefore, ellipsometry was used as a calibration for the shifts in the SPR angle or intensity. Comparison of numerous angle shift and thickness measurements gives a calibration factor of ∼14.5 nm deg^{-1}.

In addition to the MUA layers, the various other surface combinations were measured and the results tabulated in Table 1. The three different monolayers exhibited comparable thicknesses of 1.61, 1.68, and 1.58 nm for MUA, MUL and MUN on gold. These thicknesses are similar to those reported in the

(42) Stendal, A.; Beckers, U.; Wilbrandt, S.; Stenzel, O.; von Borczyskowski, C. *J. Phys. B: At., Mol. Opt. Phys.* **1996**, *29*, 2589−2595.
(43) Richter, E. M.; Augelli, M. A.; Kume, G. H.; Mioshi, R. N.; Angnes, L. *Fresenius J. Anal. Chem.* **2000**, *366*, 444−448.
(44) Sullivan, T. P.; Huck, W. T. S. *Eur. J. Org. Chem.* **2003**, 17−29.
(45) Witt, D.; Klajn, R.; Barski, P.; Grzybowski, B. A. *Curr. Org. Chem.* **2004**, *8*, 1763−1797.
(46) Schaeferling, M.; Schiller, S.; Paul, H.; Kruschina, M.; Pavlickova, P.; Meerkamp, M.; Giammasi, C.; Kambhampati, D. *Electrophoresis* **2002**, *23*, 3097−3105.
(47) Patel, N.; Davies, M. C.; Hartshorne, M.; Heaton, R. J.; Roberts, C. J.; Tendler, S. J. B.; Williams, P. M. *Langmuir* **1997**, *13*, 6485−6490.
(48) Bain, C. D.; Troughton, E. B.; Tao, Y. T.; Evall, J.; Whitesides, G. M.; Nuzzo, R. G. *J. Am. Chem. Soc.* **1989**, *111*, 321−335.

Table 1. SPR and Ellipsometric Results for Various Films

surface	SPR shift in minimum angle versus Au (deg)	differential SPR shifts for topmost layer (deg)	total film thickness from ellipsometry (nm)	thickness of topmost layer from ellipsometry (nm)
Au/MUA	0.13	0.13	1.61	1.61
Au/MUL	0.14	0.14	1.68	1.68
Au/MUN	0.15	0.15	1.58	1.58
Au/MUA/NHS	0.20	0.07	1.76	0.15
Au/BSA[a]	0.28	0.28	3.13	3.13
Au/MUL/BSA[a]	0.18	0.04	2.14	0.46
Au/MUN/BSA[a]	0.24	0.09	2.59	1.01
Au/MUA/NHS/BSA	0.40	0.20	5.54	3.78
Au/MUA/BSA	0.16	0.02	2.06	0.27

[a] Results for Au, MUL, and MUN surfaces exposed to the NHS/EDC treatment are indistinguishable from those reported here.

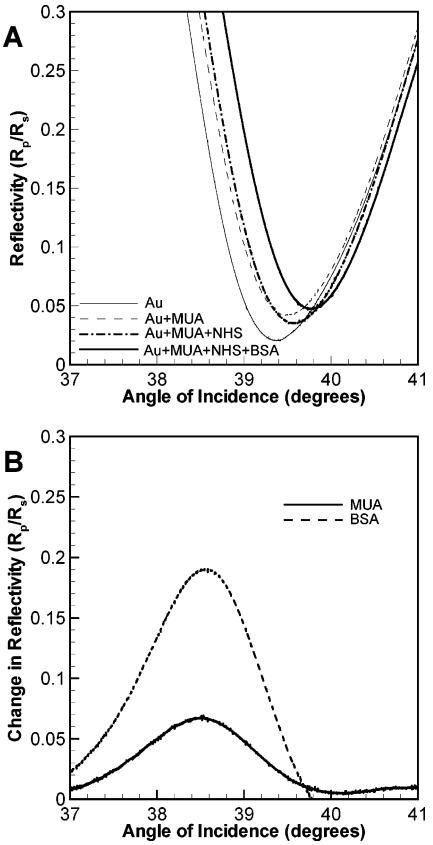

Figure 4. (A) SPR curves recorded for clean gold grating (solid line) and after subsequent surface modifications viz. MUA monolayer (dashed line), NHS esterification of MUA (dash−dot line), and covalent attachment of BSA (bold solid line). (B) Differential increase in reflectivity after MUA SAM formation (solid line) and covalent attachment of BSA (dashed line) with respect to clean gold grating.

literature for densely packed thiolate monolayers formed out of ethanolic solutions.[48,49] Treatment of the MUA surface with NHS produced a small thickness change of 0.15 nm. Similar treatment of the MUL, MUN, and bare gold surfaces produced no distinguishable change in the film thicknesses. Exposure of the various surfaces to BSA resulted in a range of responses. The largest change was observed on NHS-activated MUA with a measured film thickness of 3.78 nm after BSA exposure. This thickness is similar to those reported in the literature[50,51] and agrees well with the 14 × 4 × 4 nm ellipsoidal shape of BSA.[52] This result is also consistent with the idea that carboxylic acid groups that have been "activated" via NHS treatment will covalently bind amine moieties in the BSA structure. Notably, in the absence of NHS treatment, the BSA film thickness reached a value of only 0.27 nm on MUA. The thickness of BSA on the other surfaces was less than that on NHS-activated MUA. The bare gold surface showed large amounts nonspecific adsorption with a measured film thickness of 3.13 nm. Nonspecific adsorption of BSA was significantly lower on MUN and MUL surfaces (Table 1) with film thicknesses of 1.01 and 0.46 nm. It should be noted that submonolayer ellipsometric film thicknesses can be interpreted as incomplete film formation on the surface. Our results are consistent with literature reports describing reduced adhesive forces between BSA and hydrophilic (OH, NH_2, COOH) thiolate SAMs[53] and, as a result, lower nonspecific interactions.[54] This reflects the ability of BSA to readily participate in nonspecific adsorption onto various surfaces.

In variable-angle SPR, the resonance minimum is readily extracted and can be interpreted in terms of a thickness change. In contrast, SPR imaging typically records changes in intensity at a fixed angle of incidence. To choose the optimum angle for SPR imaging, relative changes in intensity were evaluated as a function of angle of incidence (Figure 4B). The maximum change in intensity for both the attachment of MUA on gold and further modification with BSA occurs at ∼38.5°. This angle roughly corresponds to the inflection point in the descent of the reflectivity curve as the minimum is approached from lower angles. SPR imaging at this angle should provide the highest degree of contrast with changing thickness, which should optimize the sensitivity of film thickness measurements.

Samples for SPR imaging consisted of an array of spots constructed from MUA, MUL, or MUN by printing onto the grating surface (Figure 5). Printing was achieved by "inking" a solid floating pin with a glycerol solution containing the molecule of interest and contacting the surface at a specified location (Figure 5A). Variables that influenced the size and quality of the printed spot included the pin size, the immersion depth, and the time in

(49) Porter, M. D.; Bright, T. B.; Allara, D. L.; Chidsey, C. E. D. *J. Am. Chem. Soc.* **1987**, *109*, 3559−3568.
(50) He, X. M.; Carter, D. C. *Nature* **1992**, *358*, 209−215.
(51) Brynda, E.; Houska, M. *J. Colloid Interface Sci.* **1996**, *183*, 18−25.
(52) Peters, T. *Adv. Protein Chem.* **1985**, *37*, 161−245.
(53) Kidoaki, S.; Matsuda, T. *Langmuir* **1999**, *15*, 7639−7646.
(54) Silin, V.; Weetall, H.; Vanderah, D. J. *J. Colloid Interface Sci.* **1997**, *185*, 94−103.

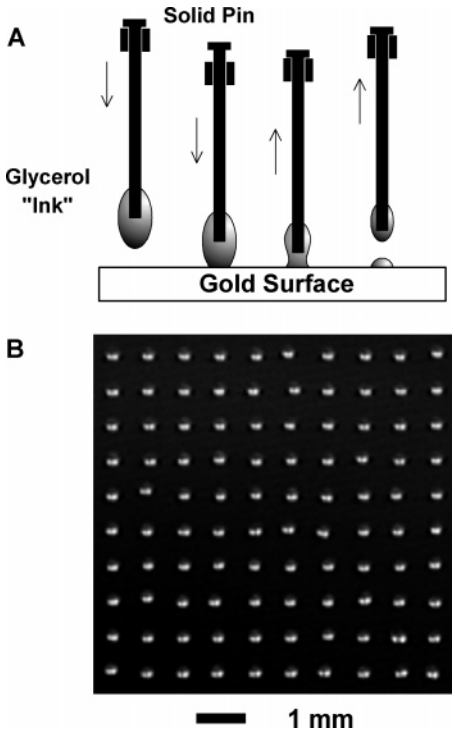

Figure 5. (A) A schematic showing the printing of MUA containing glycerol droplets. (B) Optical image showing 10 × 10 array of glycerol droplets containing thiol molecules printed in 7 mm × 7 mm region of gold. The separation between the droplets is 0.7 mm along the rows and columns.

contact with the surface. An example array is depicted in Figure 5B, which consists of a 10 × 10 array of 100 glycerol droplets containing MUA with a row and column spacing of 0.8 mm. Generally, the printed droplets showed slight spreading and elongation in a direction parallel to ridges on the grating. Arrays of various sizes and density could be readily prepared by modification of the printing routine. After a contact time of ~15 min, the glycerol droplets were then rinsed from the surface to leave behind an array of spots containing the covalently linked alkanethiol monolayers.

Glycerol was used as a solvent for printing for several reasons. The high viscosity and low evaporation rate compared to ethanol, which is typically used to prepare self-assembled monolayers, made it a desirable solvent for printing. These properties minimized droplet spreading and also prevented the droplet from evaporating before a dense monolayer had formed. The low amount of spreading allowed dense arrays to be fabricated. In addition, glycerol provided sufficient solubility to the alkanethiols of interest to allow delivery to the surface in a small droplet. The rapid kinetics of alkanethiolate monolayer formation[55] also encouraged us to try glycerol. Although the formation rate appears slower in glycerol than in ethanol, a fairly high SAM coverage occurred after a relatively short (~15 min) exposure time. Notably, a somewhat lower coverage and less well-packed monolayer might be desirable for biosensing due to the reduced steric hindrance. Indeed, mixed SAMs containing long and short alkanethiols have proven most effective for protein immobilization.[47] A short adsorption time can also help minimize multilayer formation onto the gold surface.[56]

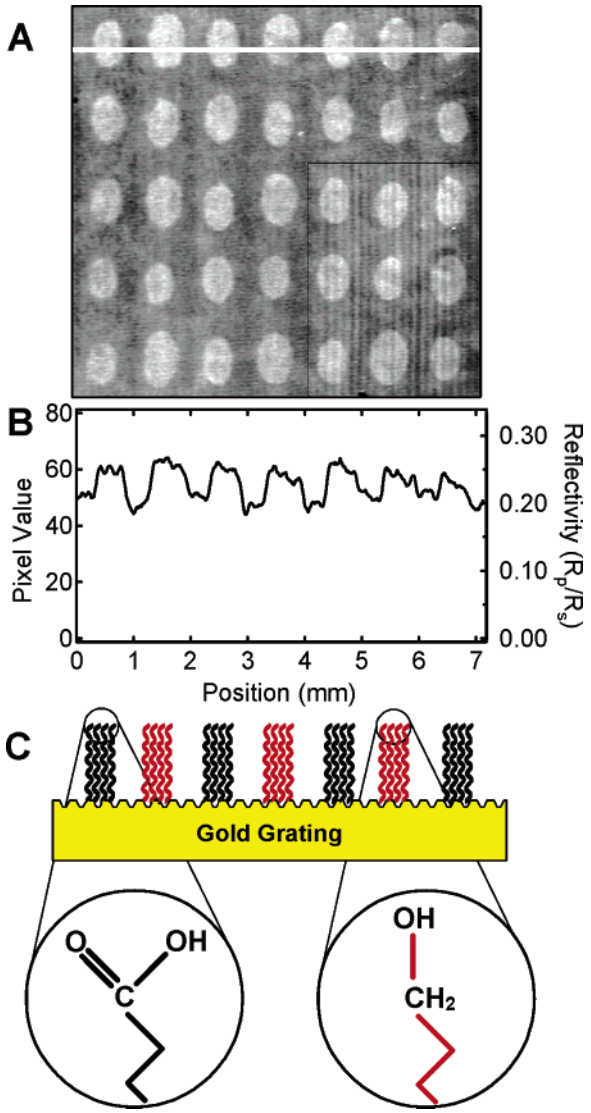

Figure 6. (A) FFT-corrected SPR intensity image of a sensor chip containing 5 × 7 array of alternating MUA and MUL spots. MUA is the first spot in the upper left and all subsequent spots down the rows and columns alternating between MUL and MUA at a spacing of ~1 mm. The outlined region in the lower right of the figure depicts the interference fringes present in the raw data. (B) Line profile of reflected intensity (R_p/R_s) along topmost row of spots. (C) Schematic showing alternating regions of MUA and MUL on gold-coated grating.

SPR images of the grating arrays were acquired by collecting the reflected light intensity (R_p/R_s) over the sample surface at a fixed angle of incidence and a single wavelength with the grating orientation perpendicular to the light path. The angle of incidence was chosen to be slightly smaller than the minimum angle for the substrate (vide supra) in order to provide maximum sensitivity for thickness changes.[8] The size of the imaging region was small enough (~7 × 7 mm) that the influence of grating curvature on the optical response was minimal. A white light source combined with a narrow band-pass interference filter having a central wavelength of 632 nm and a fwhm of 10 nm was chosen for imaging. Notably, the use of a white light source with a band-pass filter helps eliminate the interference fringes commonly observed in SPR images obtained with a laser light source without

(55) Karpovich, D. S.; Blanchard, G. J. *Langmuir* **1994**, *10*, 3315−3322.

(56) Kim, Y. T.; McCarley, R. L.; Bard, A. J. *Langmuir* **1993**, *9*, 1941−1944.

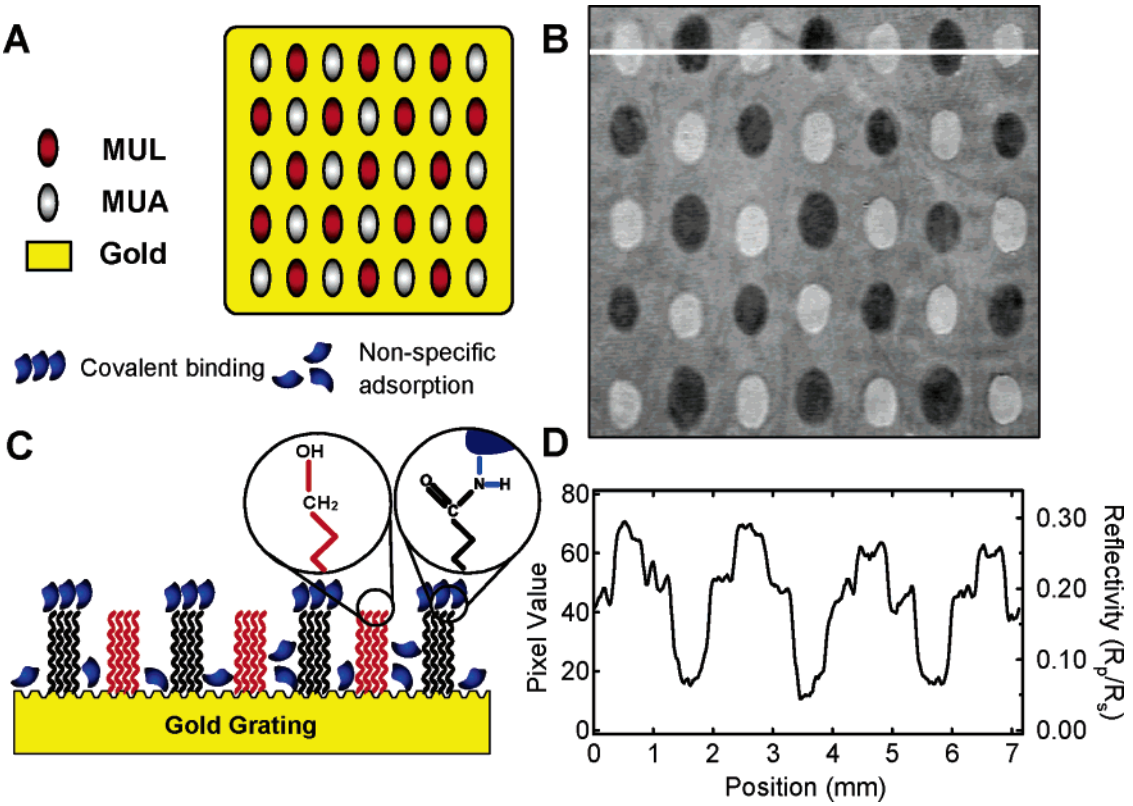

Figure 7. (A) Schematic of sensor chip depicting alternating spots of MUA and MUL on gold grating. (B) FFT-corrected SPR difference image showing reflected intensity after immobilization of BSA. The dark spots represent MUL, and the light spots are MUA after exposure the BSA. (C) Schematic depicting immobilization of BSA at various surface regions (not drawn to scale). (D) Line profile of reflected intensity (R_p/R_s) along topmost row of spots.

significant loss of sensitivity when compared to the monochromatic source.[8] Indeed, it has been shown that using a 820-nm light source with a 12-nm fwhm does not significantly degrade the quality of SPR images in prism-based sensing platforms compared to a monochromatic light source.[57]

Figure 6A depicts an SPR image of a 5 × 7 array of alternating MUA and MUL spots on a gold grating at a 38.5° angle of incidence. This image indicates the successful arraying of the gold surface with MUA and MUL spots. The spot sizes are ~0.3 mm^2 and the spacing between spots is ~1 mm. Images were captured using both p- and s-polarized light and the pixel values were divided to produce normalized (R_p/R_s) intensity images. The intensity change across a given row of spots shows a variation between gold and monolayer regions (Figure 6B). The MUA and MUL spots are indistinguishable in the image. The monolayer regions show an increase in intensity of R_p/R_s ~0.07 over the gold regions. This intensity change is consistent with that observed in variable-angle SPR (Figure 4B) and with the fact that the MUA and MUL layers are of comparable heights (Figure 6C). The detection limit of this imaging scheme can be surmised from the noise level depicted in Figure 6B at R_p/R_s ~0.01, which corresponds to a height change of ~0.25 nm. On the other extreme, saturation of the CCD imaging camera would occur at a film thickness (assuming a linear response) of ~10 nm. However, these numbers could potentially be improved with better optics and a higher quality detector. The spots in Figure 6A also present a somewhat distorted oval shape. This shape is partly due to droplet spreading along the grating ridges (down the columns). Also, since the images were acquired at an angle of 38.5°, the widths of the spots in the horizontal direction appear shorter by a factor of sin 38.5°.

All raw images captured using p-polarized light showed a light and dark band artifact (similar to interference fringes) as depicted in the inset of Figure 6A. These bands appear parallel to the grating ridges, but their origin is unclear. To reduce the impact of these bands upon the analyzed data, a fast-Fourier transform (FFT) was performed and the frequencies associated with the bands were removed. An inverse transform was then applied to yield the final images used for analysis. The filtering procedure did not degrade the image quality in any other way.

The ability of this array to adsorb the protein BSA was subsequently interrogated. The surface was first modified with NHS in order to activate the carboxylic acid groups on MUA to give it a high affinity for bonding to the amine groups in BSA. Although the entire array surface was exposed to the NHS solution, only the carboxylic acid-terminated MUA regions were modified. Figure 7B shows the SPR intensity image of the sensor chip after activation with NHS/EDC and immersion in BSA solution. The raw SPR image was subtracted from Figure 6A to present a difference image, where dark regions reflect little change while light regions reflect a large increase in intensity, which is presumably due to BSA binding. A schematic of this surface that identifies the various surface regions is shown in Figure 7A. The SPR image clearly shows that BSA interacts differently with gold,

(57) Melendez, J.; Carr, R.; Bartholomew, D.; Taneja, H.; Yee, S.; Jung, C.; Furlong, C. *Sens. Actuators, B* **1997**, *39*, 375−379.

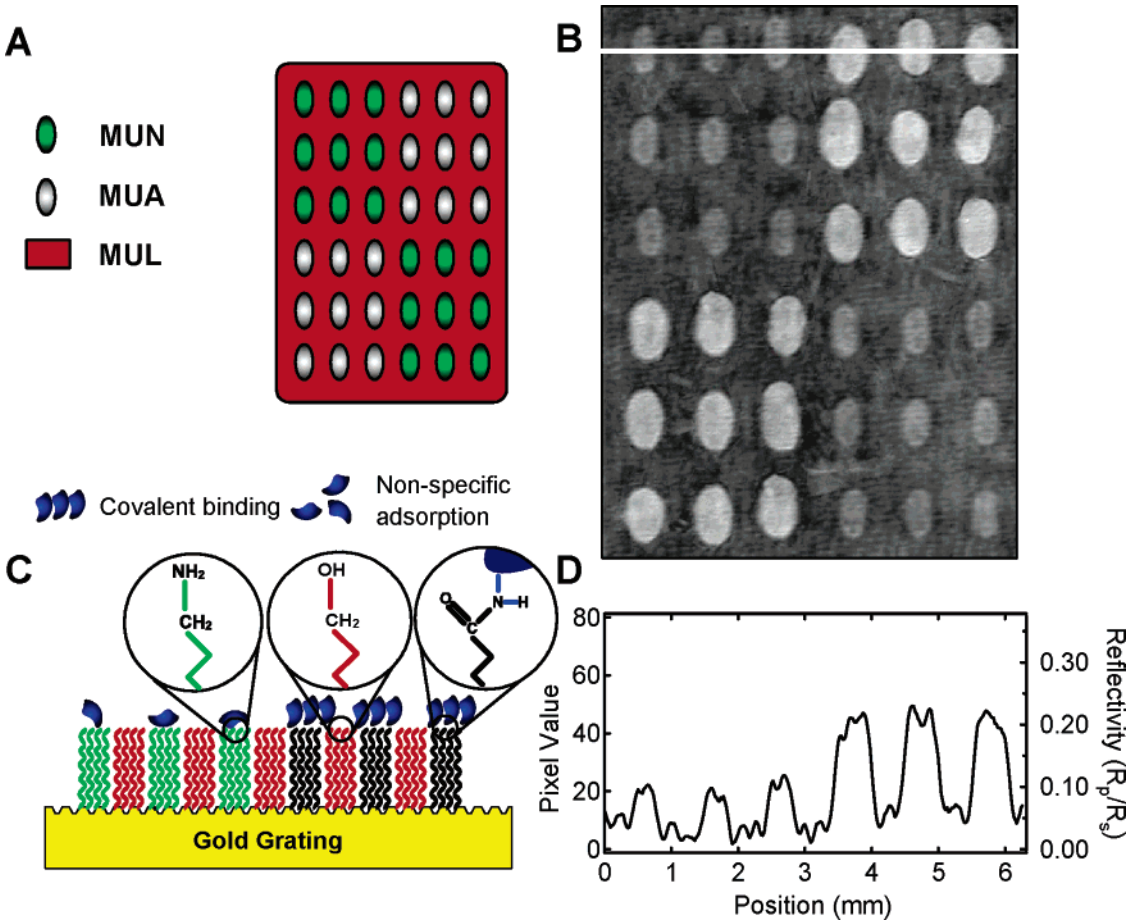

Figure 8. (A) Schematic of sensor chip depicting spots of MUA and MUN on MUL-coated gold grating. The upper left and lower right quadrants contain MUN spots while the upper right and lower left contain MUA. (B) FFT-corrected SPR difference image showing reflected intensity after immobilization of BSA. (C) Schematic depicting immobilization of BSA on MUA, MUN and MUL regions. (D) Line profile of reflected intensity (R_p/R_s) along topmost row of spots.

the OH-terminated surface of MUL, and the NHS-activated surface of MUA. In Figure 7B, the bright spots correspond to BSA covalently bound to MUA. The dark spots are MUL and their low intensity reflects minimal adsorption of BSA. The background is intermediate in brightness, which suggests substantial nonspecific adsorption of BSA on the gold surface, although not as much as that seen on MUA. A line profile of topmost row of spots (Figure 7D) shows the variation in reflected intensity along the gold substrate and alternating spots of MUA and MUL. The increase in intensity for MUL is ~0.05, for gold it is ~0.2, while for MUA is ranges between 0.26 and 0.29. A schematic of the proposed surface adsorption is given in Figure 7C. The large change in reflected intensity on MUA regions is considered to be due to the strong binding between the amine groups on BSA and the activated carboxylic acid sites. Notably, binding of BSA on MUA that was not modified by NHS treatment was very limited (Table 1). A reduced intensity is observed for BSA binding on gold, but it shows a sufficient magnitude to indicate a strong interaction between BSA and the substrate. It is unlikely that gold undergoes covalent binding with BSA, but the nonspecific interactions are large enough to create a fairly dense layer. The small change in SPR intensity at the MUL regions reflects the ability of this hydroxyl-terminated surface to substantially reduce nonspecific adsorption of BSA.

A further example of the utility of this printing method and SPR imaging on functionalized grating surfaces is illustrated in Figure 8. In this sample, a 6 × 6 array of spots containing MUA and MUN was created in a pattern in which the upper right and lower left quadrants of spots consist of MUA while the upper left and lower right are MUN (Figure 8A). MUL is then used to fill the regions between the spots to provide a background that inhibits BSA binding as compared to unmodified gold. Activation of the MUA regions is again accomplished using NHS treatment. This is followed by exposure of the surface to BSA. A SPR difference image of the resulting surface is shown in Figure 8B. The image shows three levels of contrast. The background displays a low reflected intensity, consistent with limited BSA adsorption onto the MUL-coated regions. The remaining spots show two distinct levels of contrast. The upper left and lower right quadrants, which contain MUN spots, display an intermediate brightness while the MUA spots in the upper right and lower left are much brighter. An intensity profile across the uppermost row of spots (Figure 8D) shows the quantitative intensity differences. The SPR intensity on MUA increases by ~0.23, MUN by ~0.8, and MUL by 0.03. These differences are interpreted by the schematic in Figure 8C, which shows a high BSA coverage on MUA, intermediate adsorption at MUN and essentially no adsorption on MUL. These results are consistent with what was observed

in the variable-angle SPR and ellipsometry results, which indicated weak BSA binding at MUL, strong binding at MUA, and intermediate binding at MUN.

Figures 7 and 8 represent just two examples of the range of surface patterns and chemistries that can be prepared and evaluated in this manner. In principle, one could substantially increase the number of spots in these printed arrays, with the primary limitations being the size of the imaging window and the minimum spacing between spots. Our current SPR imaging system allows a maximum image window of 1-in. diameter due to the size of the imaging optics. This image window could be increased by using larger lenses. At present, our printing system allows a minimum droplet spacing of ~0.7 mm to avoid merging of the printing droplets. This spacing would allow an array of ~225 spots cm^{-2} to be constructed. In principle, the chemistry of each spot could also be different or consisting of various chemistries with numerous replicas.

CONCLUSIONS

We have described a simple and inexpensive, yet robust and flexible sensor platform based upon surface plasmon resonance imaging of a grating surface. The results indicate a highly sensitive detection scheme that is highly quantitative to film formation down to fractions of a monolayer. It has been demonstrated that prism- and grating-based SPR coupling methods give comparable theoretical sensitivities for angular interrogation modes.[58] However, there are several advantages of using grating-based SPR sensing. There is no need for expensive glass components (prisms, slides) or index-matching fluid. Minimal alignment of optics is required, which imparts robustness to grating-based sensing. In addition, the sensor chip is mass-producible using the same inexpensive injection molding technology that is the state of the art for production of compact disks. Although commercially available CD-Rs provide a somewhat limited selection of grating periods and amplitudes, one could readily fabricate other sizes and shapes using standard photolithography and etching techniques.

In this work, we have focused on the development of a sensor platform that utilizes ex situ detection in air after exposure to a solution of interest. This format simplifies the optics required for readout of the detector response. However, one could readily adapt a grating substrate for in situ detection by fabricating a cell with optical windows at the appropriate viewing angles. The primary disadvantages of this approach would be the added complexity and the attenuation experienced by the light as it travels through the solvent.

The ability to construct arrays via pin printing of various surface chemistries allows complex sensor platforms to be easily created. The pin printing we have described allows a range of chemistries and array structures to be constructed with high reproducibility. Although this type of contact printing has some limitations when compared to jetted printing, its robustness and simplicity provides clear advantages. Indeed, pin printing systems are commonly used in the manufacture of protein microarrays and numerous printing tools are commercially available.[59−62] In addition, the pin printing described here could be easily performed on any variety of surfaces and is not limited to the gratings substrates we used.

We have demonstrated the performance and utility of this method using a selection of functionalized self-assembled monolayers for the adsorption of BSA. This technique could be easily expanded and adapted to a variety of more complex surface chemistries as well as being readily applied to additional proteins and complex biomolecules.

ACKNOWLEDGMENT

The authors gratefully acknowledge the National Science Foundation (CTS-0405442) and Iowa State University for partial support of this work.

SUPPORTING INFORMATION AVAILABLE

Variable-angle surface plasmon resonance curves and ellipsometry data for the various surfaces and films. This material is available free of charge via the Internet at http://pubs.acs.org.

Received for review October 27, 2005. Accepted December 21, 2005.

AC0519209

(58) Homola, J.; Koudela, I.; Yee, S. S. *Sens. Actuators. B* **1999**, *54*, 16−24.

(59) Zhu, H.; Bilgin, M.; Bangham, R.; Hall, D.; Casamayor, A.; Bertone, P.; Lan, N.; Jansen, R.; Bidlingmaier, S.; Houfek, T.; Mitchell, T.; Miller, P.; Dean, R. A.; Gerstein, M.; Snyder, M. *Science* **2001**, *293*, 2101−2105.

(60) Arenkov, P.; Kukhtin, A.; Gemmell, A.; Voloshchuk, S.; Chupeeva, V.; Mirzabekov, A. *Anal. Biochem.* **2000**, *278*, 123−131.

(61) Lueking, A.; Horn, M.; Eickhoff, H.; Bussow, K.; Lehrach, H.; Walter, G. *Anal. Biochem.* **1999**, *270*, 103−111.

(62) MacBeath, G.; Schreiber, S. L. *Science* **2000**, *289*, 1760−1763.